PHYSICAL REVIEW B **72**, 205104 (2005)

Combined theoretical and experimental study of the low-temperature properties of $BaZrO_3$

A. R. Akbarzadeh,[1] I. Kornev,[1] C. Malibert,[2,3] L. Bellaiche,[1] and J. M. Kiat[2,4]
[1]*Physics Department, University of Arkansas, Fayetteville, Arkansas 72701, USA*
[2]*Laboratoire Structures, Propriétés et Modélisations des Solides, Ecole Centrale Paris, 92295 Châtenay-Malabry Cedex, France*
[3]*Laboratoire d'Etudes des Milieux Nanométriques, Université d'Evry Val d'Essonne, 91000 Evry, France*
[4]*Laboratoire Léon Brillouin, CE Saclay, 91191 Gif-sur-Yvette Cedex, France*

(Received 11 March 2005; revised manuscript received 8 August 2005; published 2 November 2005)

Low temperature properties of $BaZrO_3$ are revealed by combining experimental techniques (x-ray diffraction, neutron scattering and dielectric measurements) with theoretical first-principles-based methods (total energy and linear response calculations within density functional theory, and effective Hamiltonian approaches with and without zero-point vibrations). Unlike most of the perovskite systems, $BaZrO_3$ does not undergo any (long-range-order) structural phase transition and thus remains cubic and paraelectric down to 2 K, even when neglecting zero-point vibrations. On the other hand, these latter pure quantum effects lead to a negligible thermal dependency of the cubic lattice parameter below $\simeq$40 K. They also affect the permittivity of $BaZrO_3$ by inducing an overall saturation of the real part of the dielectric response, for temperatures below $\simeq$40 K. Two fine structures in the real part, as well as in the imaginary part, of the dielectric response are further observed around 50–65 K and 15 K, respectively. Microscopic origins (e.g., unavoidable defects and oxygen octahedra rotation occurring at a local scale) of such anomalies are suggested. Finally, possible reasons for the facts that some of these dielectric anomalies have not been previously reported in the better studied $KTaO_3$ and $SrTiO_3$ incipient ferroelectrics are also discussed.

DOI: 10.1103/PhysRevB.72.205104 PACS number(s): 77.22.Gm, 61.50.−f, 61.10.Nz, 61.12.Ex

I. INTRODUCTION

$BaZrO_3$ is a ceramic oxide of the perovskite family structure with a large lattice constant, high melting point, small thermal expansion coefficient, low dielectric loss and low thermal conductivity (see, e.g., Refs. 1–13 and references therein). These aforementioned properties make $BaZrO_3$ (i) a very good candidate to be used as an inert crucible in crystal growth techniques,[7,11] (ii) an excellent material for wireless communications[1,10] and (iii) a very good substrate in thin film deposition.[1,3] $BaZrO_3$ is also one of the two parent compounds of the (Pb-free and thus environmental-friendly) $Ba(Zr,Ti)O_3$ solid solutions, which is promising for manufacturing high Q materials with a variety of applications in microwave industry.[13]

Interestingly, properties of $BaZrO_3$ have been measured as long as 40 years ago, as well as very recently,[1–3] but only at room or higher temperature (to the best of our knowledge). Similarly, we are not aware of any calculation (either from phenomenological theory or first-principles calculations) predicting the dielectric properties of $BaZrO_3$. As a result, low-temperature dielectric properties of $BaZrO_3$ have never been investigated, despite the fact that many unusual effects are known to occur in some perovskite materials between 0 and 50 K. One drastic example of such effects is the (temperature-independent) plateau and large values of the real part of the dielectric response in $KTaO_3$ and $SrTiO_3$, which arise from the quantum-induced suppression of ferroelectricity in these materials. Other examples are the anomalous peaks observed around 10-50 K for the imaginary part of the dielectric response in $KTaO_3$, $K(Ta,Nb)O_3$, $(Pb,La)TiO_3{:}Cu$,[14,15] and $SrTiO_3$,[15,16] that are neither associated with structural phase transition nor do have a corresponding peak in the real part of the dielectric response (which conflicts with the well-established Kramers-Kronig relations[17]).

The aim of this article is to investigate the low-temperature behavior of $BaZrO_3$ from measurements and first-principles-based simulations. We report several unusual features in the real and imaginary parts of the dielectric responses while *no* long-range ferroelectric, antiferroelectric or antiferrodistortive structural phase transition occurs in $BaZrO_3$ down to 2 K. Discussions and similarities or differences between $BaZrO_3$ and the (better-studied) $KTaO_3$ and $SrTiO_3$-related materials are also indicated to better understand the low-temperature dielectric anomalies reported in several perovskites.

This article is organized as follows. Section II describes the experimental and theoretical methods we used to investigate $BaZrO_3$. Section III reports the measurements and predictions for structural and dielectric properties. Finally, Secs. IV and V provide a discussion and conclusion, respectively.

II. METHODOLOGY

A. Experimental procedures

Powder samples of $BaZrO_3$ were synthesized by solid state reaction by calcination at 1400 K and sintering at 1600 K starting from stoichiometric amounts of the corresponding oxides ($BaCO_3$, ZrO_2). The synthesized samples were well crystallized and no presence of parasitic phases was evidenced by x-ray diffraction (XRD) and chemical analysis. The final fired density is around 88–90 %, the typical grain size is $\simeq$10 μm and the size distribution is typically 10% of the mean grain size. The temperature dependence of the di-

TABLE I. The LDA-derived H_{eff} parameters in atomic units for BaZrO_3, at its low-temperature experimental lattice constant, following the notations of Ref. 29.

Lattice constant	a_0	7.91943	Soft mode mass	75.721		
Onsite	κ_2	0.0183	α	0.009733	γ	0.01663
	j_1	−0.00738	j_2	0.02311		
Intersite	j_3	0.00262	j_4	−0.00163	j_5	0.00120
	j_6	0.00049	j_7	0.00024		
Elastic	B_{11}	4.794	B_{12}	0.755	B_{44}	1.416
Soft mode elastic	B_{1xx}	−0.431	B_{1yy}	0.033	B_{4yz}	−0.055
Dipole	Z^*	5.81	ε_∞	4.928		

electric constant was measured at various frequencies in a temperature range from 5 K to 300 K using a Hewlett-Packard 4192A impedance analyzer and a cryostat with an estimated precision of 0.1 K. These measurements were performed on ceramic samples which were polished and cleaned, and sputtered gold electrodes were applied. Samples were annealed at 800 K and slowly cooled in order to eliminate strains caused by polishing. Powdered samples were used for the diffraction experiments. X-ray-diffraction measurements were performed on a high accuracy, two-axis diffractometer in a Bragg-Brentano geometry using Cu-Kb wavelength issued from a 18-kW rotating anode generator, with diffraction angles precision better than 0.002 deg. The neutron powder diffraction patterns were collected at temperatures between 300 and 2 K on the 3T2 high resolution goniometer on a thermal source (1.227 Å) using the Orphe reactor facilities at Laboratoire Léon Brillouin (Saclay, France). Structural Rietveld refinements on both x-ray and neutron patterns were carried out with the XND software.

B. Theoretical approaches

In this study, two different (direct) first-principles codes, as well as a first-principles-derived technique, were used to obtain and/or extract various information.

One of the two first-principles codes is denoted ABINIT.[18] We took advantage of its implementation of the linear response theory to compute the phonon dispersion curves of BaZrO_3 at its low-temperature experimental lattice constant. Some technical details are as following. In this method we used Teter extended norm-conserving pseudopotentials[19] and the local-density approximation (LDA).[20] The exchange-correlation functional was approximated using Perdew-Zunger parametrization[21] of Ceperley-Alder data.[22] The Ba $5s^2$, Ba $5p^6$, Ba $6s^2$, Zr $4s^2$, Zr $4p^6$, Zr $4d^2$, Zr $5s^2$, O $2s^2$, and O $2p^6$ electrons are treated as valence electrons. A plane-wave cut off of 100 Ry was used to obtain convergence of the ground state total energy. Phonon frequencies were found to converge for dynamical matrices calculated on a $6\times6\times6$ Monkhorst-Pack grid.[23]

The second first-principles code used in our study is denoted CUSP.[24] It also implements the LDA,[20] and the Ceperley-Alder exchange and correlation[22] as parametrized by Perdew and Zunger.[21] We also used the same valence electrons (indicated above) as in the ABINIT code. On the other hand, the pseudopotentials are those given by the Vanderbilt ultrasoft scheme,[25] and the plane-wave cutoff is chosen to be 25 Ry, which leads to converged results of physical properties of interest.[24] The CUSP code is used to calculate the energetics of BaZrO_3 that are associated with the rotation of the oxygen octahedra, at its low-temperature experimental lattice constant. It is also used to derive, at this specific lattice constant, the 18 parameters of the first-principles-based effective Hamiltonian (H_{eff}) approach developed in Ref. 26. These parameters are given in Table I.

We also perform simulations using such H_{eff} technique (and its parameters) to go beyond the abilities of direct first-principles techniques, namely to investigate *finite-temperature* properties of large BaZrO_3 supercells. The degrees of freedom of this Hamiltonian are the so-called local modes (that are directly proportional to the spontaneous electrical polarization), and the strain variables (that characterize the crystallographic phase). The total energy, E_{tot} of H_{eff} contains five different interactions between local modes and/or strains, namely, a local-mode self energy, a long-range dipole-dipole interaction, a short-range interaction between local modes, an elastic energy and an interaction between local-modes and strain.[26] Monte Carlo (MC) simulations are performed using E_{tot} in two different schemes: classical Monte Carlo (CMC),[27] which neglects zero-point vibrations and, path-integral quantum Monte Carlo (PI-QMC),[28–30] which includes these quantum-mechanical zero-point motions. Consequently, comparison between the results of these two different Monte Carlo techniques will allow the determination of quantum effects on structural and dielectric properties of BaZrO_3. $12\times12\times12$ supercells (corresponding to 8 640 atoms) are used in all Monte Carlo simulations. We typically perform 30 000 MC sweeps to thermalize the system and 70 000 more to compute averages, except at low temperatures in PI-QMC where more statistics is needed.

In PI-QMC, each 5-atom cell interacts with its images at neighboring imaginary times through a spring-like potential (representing the zero-point vibrations as implemented in PI-QMC formulations), while all the 5-atom cells interact with each other at the same imaginary time through the internal potential associated with E_{tot}. The product TP, where T is the simulated temperature and P is the number of imaginary time slices, controls the accuracy of the PI-QMC calculation.[31] In all our simulations we use $TP=600$, which we find leads to sufficiently converged results. Outputs of the

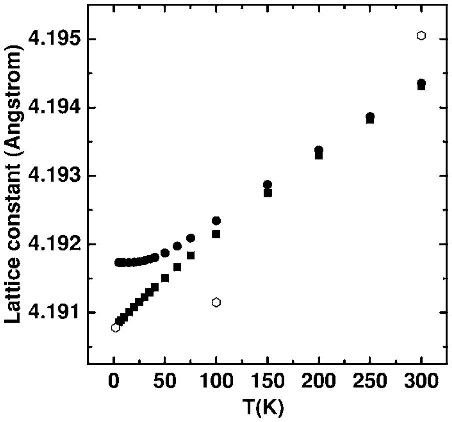

FIG. 1. Evolution of the cubic lattice constant as a function of temperature in $BaZrO_3$. Solid squares and solid circles correspond to the CMC and PI-QMC predictions, respectively, while the open symbols display the results of neutron scattering. Note that the CMC predictions exactly agree with the experimental data at low temperature as a consequence of our choice of the a_0 parameter for the effective Hamiltonian approach (see Table I).

PI-QMC simulations thus contain local modes $\mathbf{u}_i(t)$, where i runs over the 5-atom unit cells of the studied supercell while the imaginary time t ranges between 1 and P. (Note that $t=P=1$ corresponds to CMC simulations.) Strain variables are another output of MC simulations.

III. RESULTS

A. Structural properties

XRD and neutron scattering indicate that $BaZrO_3$ is cubic (and thus paraelectric) down to 2 K (the minimal temperature accessed during our neutron scattering). Note that we are not aware of any previous measurement investigating the low-temperature, rather than high-temperature,[2,3,32] properties of $BaZrO_3$.

Our experimental result is consistent with the fact that we further find that our PI-QMC simulations using the effective Hamiltonian approach provide a vanishing supercell average of the local-modes down to 0 K and a resulting cubic ground-state. Interestingly, our CMC simulations also predict such paraelectric ground-state. This indicates that, unlike $KTaO_3$[33,34] and $SrTiO_3$[16,29] for which quantum effects suppress ferroelectricity in favor of paraelectricity, zero-point phonon vibrations do *not* affect the symmetry of the ground-state in $BaZrO_3$. On the other hand, Fig. 1—which displays the predicted and measured temperature evolutions of the cubic lattice constant of $BaZrO_3$—clearly shows, via the comparison of CMC and PI-QMC results, how zero-point vibrations *quantitatively* affect structural properties of $BaZrO_3$. Below 100 K, the zero-point phonon vibrations tend to prevent the lattice constant from decreasing when decreasing the temperature. Quantum effects thus increase the lattice constant with respect to classical predictions, with this increase becoming more pronounced as the temperature decreases. As a matter of fact, PI-QMC calculations result in (1) a dramatic change of thermal expansion below *versus* above 100 K, (2) a lattice constant that is nearly temperature-independent below $\simeq 40$ K, and (3) a lattice parameter that is larger by 10^{-3} Å from its CMC result at the lowest temperatures. Note that item (1) is clearly confirmed by our neutron scattering data (reported in Fig. 1 for 300, 100, and 2 K) that shows a relatively rapid $\simeq 10^{-3}$ Å decrease of the lattice constant between 300 K and 100 K, while the difference in lattice parameters between 100 and 2 K is as small as 3×10^{-4} Å. Furthermore, items (1) and (2) have also previously been observed in the incipient $KTaO_3$ system[35] (but for different critical temperatures). Moreover, item (3) provides a measure of the (relatively small) quantitative effects of zero-point motion of ions on the lattice parameter *per se* (rather than on the thermal expansion) of $BaZrO_3$.

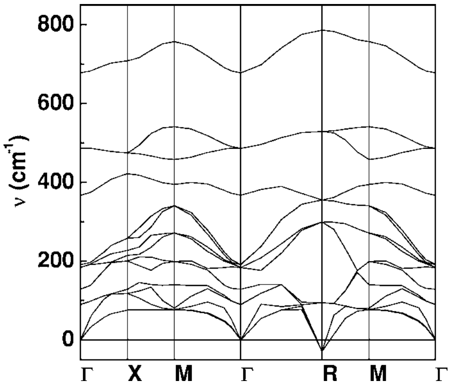

FIG. 2. Phonon dispersion of cubic $BaZrO_3$, from first principles calculations.

Figure 1 also indicates that above 100 K, one can safely use the approximation that the cubic lattice parameter *linearly* depends on temperature with the thermal expansion coefficient being $0.27\times 10^{-5}(1/K)$, $0.23\times 10^{-5}(1/K)$ and $0.47\times 10^{-5}(1/K)$ for the CMC, PI-QMC and neutron scattering data, respectively. Our experimental value of $0.47\times 10^{-5}(1/K)$ compares rather well with the linear thermal expansion coefficient of $0.69\times 10^{-5}(1/K)$ previously measured by x-ray diffraction for temperature ranging between 273 and 873 K.[36] On the other hand, the thermal expansion of $0.27\times 10^{-5}(1/K)$ and $0.23\times 10^{-5}(1/K)$ predicted by our simulations underestimate the experimental values by a ratio of 2–3. This discrepancy between simulations and the measurements arises from the fact that the effective Hamiltonian approach only incorporates the ferroelectric-related vibrations among the optical modes, while an accurate description of thermal expansion requires to take into account *all* phonon modes.[37]

The effective Hamiltonian approach used in our study thus also neglects some phonon modes that may condense in $BaZrO_3$, such as the R_{25} modes that are associated with the rotation of the oxygen octahedra.[38] To check such possibility, we decided to compute the whole phonon dispersion of cubic $BaZrO_3$ at its low-temperature experimental lattice constant, using the linear response theory as implemented in the first principles ABINIT code.[18] The results are shown in Fig. 2, and indeed confirm the previous *ab initio* prediction[38] of the condensation of the R-point zone-boundary mode. (Note that these phonon calculations also confirm that $BaZrO_3$ does not

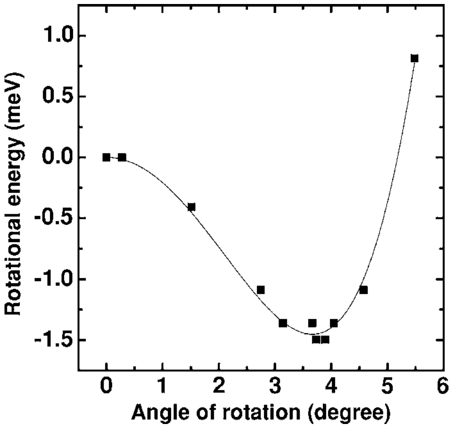

FIG. 3. Oxygen octahedra rotational energetics (per 5 atoms) *versus* the angle of the rotation about the [001] direction from first principles calculations. The zero of energy corresponds to the paraelectric state. The solid line is a guide for the eyes.

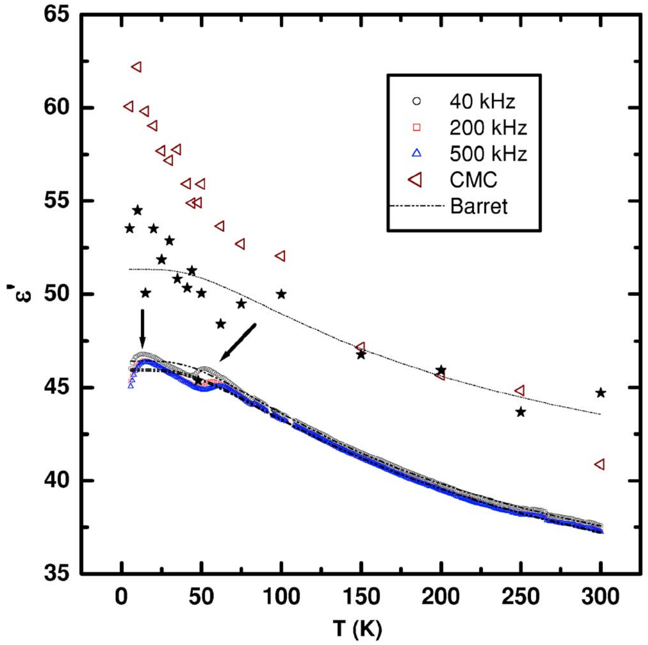

FIG. 4. (Color online) Theoretical (using CMC and PI-QMC simulations) and experimental (for different frequencies) real part of the dielectric constant. Dash-dot-dot lines show the fit of the data into the Barret relation. The arrows indicate the position of the two observed dielectric anomalies that are discussed in the text. The statistical error bars for the PI-QMC data are estimated to have a magnitude of 2.

exhibit any ferroelectric instability at the Γ point, even when quantum statistics are neglected.) One has to realize, though, that the instability associated with these antiferrodistortive motions is rather weak, as demonstrated by the relatively *small* negative value of the frequency.[39] This is further evidenced in Fig. 3, that displays the total energy (as predicted by the first principles CUSP program[24]) versus the angle of the octahedra rotation about the [001] direction: the minimum energy (occurring for an angle about 4°) is only $\simeq 1.5$ meV deeper than the energy of the paraelectric phase (associated with a zero angle). Such difference in energy corresponds to a rather small temperature of ≈ 17 K. It is thus highly possible that zero-point vibrations prevent the occurrence (down to 2 K) of the macroscopic cubic paraelectric-to-antiferrodistortive phase transition, which would explain why our low-temperature XRD and neutron scattering experiments do not reveal any additional peak related to a doubling of the unit cell. This quantum-induced suppression may act either globally (i.e., different unit cells do exhibit some rotation of their oxygen octahedra, but these rotations are not long-range correlated) or locally (i.e., there is no rotation of the oxygen octahedra in any unit cell). We will come back to this point, and to this ≈ 17 K temperature, when discussing the results on dielectric properties.

B. Real part of the dielectric response

Figure 4 shows our experimental determination of the real part of the dielectric response, ε', versus temperature for different frequencies. Our room-temperature data are around 37, independent of the frequency, and agree rather well with the previously reported value of 32 given in Ref. 40. Furthermore, the real part of the dielectric response of $BaZrO_3$ increases as the temperature decreases from 300 K for any given frequency. It then exhibits an overall low-temperature saturation to a plateau having a value that is slightly dependent on the frequency (ranging between 47 and 45 for frequencies of 40 kHz, 200 kHz, and 500 kHz, respectively). The existence of such plateau has already been reported in the incipient ferroelectrics $KTaO_3$[33,34] and $SrTiO_3$,[16,29] and is usually thought to be associated with zero-point vibrations. To check this fact, we also report in Fig. 4 the predictions from the H_{eff} approach using both CMC and PI-QMC techniques. It is obvious that using CMC, the real part of the dielectric response continuously increases to higher value when the temperature decreases, while on the other hand the dielectric constant computed within PI-QMC tends to saturate, in overall, at low-temperature.[41] Our simulations thus prove that quantum fluctuations play an important role on the low-temperature dielectric responses of $BaZrO_3$, as in $KTaO_3$[33,34] and $SrTiO_3$.[16,29] However and as already mentioned in Sec. III A, this quantum-induced modification of permittivity in $BaZrO_3$ is *not* accompanied by a suppression of ferroelectricity since $BaZrO_3$ does not have any ferroelectric instability even in the classical regime—as indicated by the fact that our CMC simulations lead to a cubic paraelectric ground state and a lack of peak in ε'. This distinguishes $BaZrO_3$ from both $KTaO_3$ and $SrTiO_3$. Figure 4 also reveals that our PI-QMC simulations yield predictions that are slightly larger in magnitude than our experimental results. In fact, this may be expected since (i) the measurements displayed in Fig. 4 demonstrate that decreasing frequency leads to an increase of the dielectric response at any temperature and (ii) the calculations correspond to the static regime, i.e., to a zero frequency. Two other possible reasons can also be invoked for the fact that the simulations yield larger ε' with respect to experiment for any temperature. First of all, one has to realize that the simulated real part of the dielectric response is quite sensitive to the used ε_∞ high-frequency dielectric constant. For instance, a decrease of ε_∞ by 5% with

TABLE II. Coefficients of the fit of the real part of the dielectric response into the Barrett relation. All the parameters of all the fits are allowed to relax, except the parameters C and T_s for the fit of the PI-QMC data that are kept frozen to their deduced values from our experiments at the lowest frequency. Such freezing is necessary to allow the fit to converge because of the relatively large fluctuation inherent to PI-QMC simulations at low temperature.

f (kHz)	40	200	500	PI-QMC
C	3214±204	3661±281	4177±369	3214
T_s (K)	81±2	81±3	78±3	81
T_0 (K)	−114±11	−135±14	−158±17	−131±25
B	29.9±0.3	29.0±0.4	28.2±0.5	30.3±0.3

respect to the LDA value of 4.928 brings the static real part of the dielectric response from a value of 51 to a value of 64 at 10 K, within PI-QMC simulations.[44] Secondly, one also has to realize that the the final fired density of our grown samples is around 90%, and thus should lead to smaller ε' than the one associated with a "perfect" sample, i.e., with a sample having a 100% density (as the one mimicked in our simulations). In fact, multiplying the experimental dielectric response ε', shown in Fig. 4 and corresponding to 10 kHz, by a corrective porosity factor of 100/90 leads to data that agree extremely well with the PI-QMC simulations. We can thus conclude that the PI-QMC results are in overall quite accurate, especially when realizing that dielectric coefficients are related to the *derivative* of the polarization (i.e., they are much more difficult to predict than properties that are directly proportional to polarization) and that the magnitude of ε' is rather small in $BaZrO_3$ (e.g., the low-temperature plateau has a value that is smaller by ≃2–3 orders of magnitude than the corresponding ones in $KTaO_3$[14,33,42] and SrTiO3[16,43]). To further analyze our results, we fitted them using the traditionally-used Barret relation[45]

$$\varepsilon' = \frac{C}{T_s \coth\left(\frac{T_s}{T}\right) - T_0} + B, \qquad (1)$$

where C and T_s are the so-called Curie constant and saturation temperature, respectively.[33,45,46] T_0 is interpreted as being the classical Curie temperature (that is, the Curie temperature if quantum effects would not exist) and B is a constant independent of temperature. The resulting fits are indicated by means of solid lines in Fig. 4, and the coefficients of these fits are given in Table II.

In addition to the fact that the quality of these fits is in overall rather good (thus, confirming, as in $KTaO_3$ and $SrTiO_3$, the relevance of the empirical Barret relation for describing quantum effects on permittivity of perovskites), four features are particularly worth noticing related to these fits. First of all, T_0 is (strongly) *negative* which confirms our theoretical findings that $BaZrO_3$, unlike $KTaO_3$ and $SrTiO_3$, does *not* exhibit any ferroelectric instability even in the classical regime. Secondly, the T_s deduced from the experimental data is around 80 K, which is located in the temperature region for which PI-QMC predictions begin to significantly differ from CMC results for dielectric as well as structural properties (see Fig. 4 and Fig. 1). In other words, our simulations confirm the physical meaning usually associated with T_s, that is the temperature below which quantum effects play a non-negligible role on physical properties.[33,45,46] Thirdly, and also unlike in $KTaO_3$[46] and $SrTiO_3$,[43] the B parameter can*not* be neglected to get good fits in $BaZrO_3$. This latter difference is due to the fact that the low-temperature plateau is much larger in $KTaO_3$ (around 4000)[14,33,42] and $SrTiO_3$ (around 20 000)[16,43] than in $BaZrO_3$ (around 46, see Fig. 4), or equivalently that T_0 is positive in $KTaO_3$[33,46] and $SrTiO_3$[43] while being negative in $BaZrO_3$. Finally, two fine structures, existing in the experimental data, deviate from (and seem to be superimposed with respect to) the Barrett fit. More precisely, one hump appears in ε' around 50 K at the lowest used frequency *versus* 65 K for the highest frequency, while a second hump shows up around 15 K for (more-or-less) any frequency. This second hump becomes more pronounced when increasing frequency. Note that these relatively small humps do *not* appear within our CMC simulations, and that the large fluctuations inherent to the PI-QMC approach[31] do not allow us to assert if these humps are also predicted from our quantum simulations.

C. Imaginary part of the dielectric response and dielectric loss

Figure 5 displays the *imaginary* part of the dielectric response, ε'' and the loss angle (as given by $\tan\delta = \varepsilon''/\varepsilon'$) of $BaZrO_3$ versus temperature for frequencies ranging between 10 kHz and 1 MHz. All the results displayed in Fig 5 are from measurements since simulating loss on an *ab initio* level is one of the most interesting and difficult challenges that remain to be accomplished nowadays. One can first notice from Fig 5 that both ε'' and $\tan\delta$ are very weak for the whole investigated frequency range, as also observed in $Ba(Zn_{1/3}Ta_{2/3})O_3$-$BaZrO_3$ solid solutions.[13] $BaZrO_3$ can thus be a material of choice to design high-Q compounds. Furthermore, our measurements show the existence of two loss anomalies, namely a peak in ε'' (and $\tan\delta$) around 45–60 K and a continuously increasing ε'' (and $\tan\delta$) when decreasing temperature below 20 K. These two anomalies are correlated with the humps seen in ε' since they occur at similar temperatures and since they behave in a similar fashion. For instance, both the peaks in ε' and ε'', occurring around 50 K at low frequency, shift to higher temperature when increasing the frequency. Similarly, the anomalies observed in ε' and ε'' at very low temperature get more pronounced at higher frequency. Interestingly, the well-known Kramers-Kronig relations[17] imply that any peak or anomaly in ε' should be accompanied with a peak or anomaly in ε'' (and vice-versa) at the same temperature. Such correlation is thus indeed satisfied in $BaZrO_3$, but surprisingly, does not seem to hold for pure SrTiO3 and KTaO3. More precisely, ε'' has been found to exhibit a peak in these two latter materials for a temperature around 30–50 K, but no corresponding peak has been seen in the real part of the dielectric response. One possible reason for this lack of observation in pure $KTaO_3$ and pure $SrTiO_3$ may be due to the fact that these two materials (unlike $BaZrO_3$) have a *large* overall real part of the dielectric

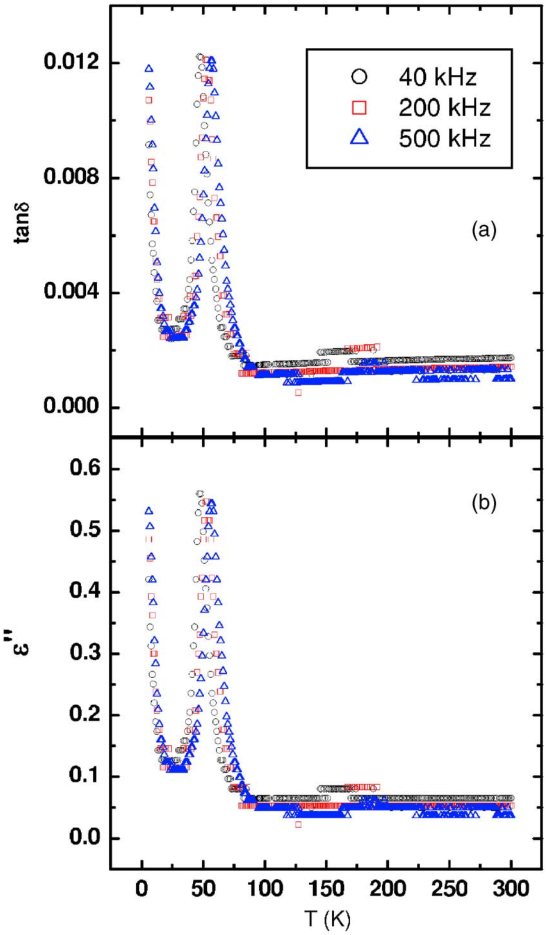

FIG. 5. (Color online) Measured (a) loss angle, tan δ, and (b) imaginary part of the dielectric response, ε'', at different frequencies *versus* temperature.

response[16,33] that "washes out" (i.e., prevents the observation of) weak superimposed peaks.

Furthermore, the dielectric anomalies seen in $BaZrO_3$ and reported in Figs. 4 and 5 are also rather intriguing since our XRD and neutron scattering do not detect any structural phase transition down to 2 K. A discussion about their possible causes is given in the next section.

IV. DISCUSSIONS

We believe that the enhancement in the real and imaginary parts of the dielectric responses occurring at temperature around $\simeq$15 K is due to the activation of the oxygen octahedra rotation in $BaZrO_3$. This belief is based on the fact that the minimum energy associated with antiferrodistortive motions is predicted to correspond to a temperature that is very close to the one at which these enhancements begin to occur, namely 17 K (see Fig. 3 and Sec. III A). The zero-point phonon vibrations may annihilate the *long-range order* of such rotation down to 2 K, which would explain our x-ray diffraction and neutron scattering results. However, these quantum-induced effects likely can not prevent the octahedra rotation from occurring at a *local* scale (especially at very low temperature), which would be consistent with the fact that ε'' increases when decreasing the temperature below 20 K (see Fig. 5).

Regarding the unusual dielectric features occurring around 50 K, it is important to realize that a frequency-dependent peak has previously been reported for tanδ and ε'' in several other perovskite systems [e.g., $BaTiO_3$:La, $SrTiO_3$:La, $SrTiO_3$,$SrTiO_3$:Ca, K(Ta,Nb)O_3, (Pb,La)TiO_3:Cu, $KTaO_3$] *near a similar temperature* (see, e.g., Refs. 14–16 and 34, and references therein). For instance, ε'' peaks around 40 K for low frequency in $KTaO_3$.[14,34] It is commonly believed that the reasons behind these peaks is the existence of unavoidable impurity ions having a different valence than the host atoms (see Refs. 47 and 48 and reference therein). In such a case, these peaks should become more pronounced when intentionally doping the sample with impurities, as consistent with the fact that adding up to 3% of Mn^{2+} in $KTaO_3$ leads to a noticeable peak in the real part of the dielectric response around 40 K.[47] Observing and understanding the effects of doping on physical properties of $BaZrO_3$ is thus of importance to confirm this (general) possibility, but goes beyond the scope of the present article. One particular previous study[15] further stipulates that it is a polaronic relaxation—that is, a coupling between the free charge carriers arising from the impurity ions and the lattice properties of the host material—that causes such weak dielectric anomalies. As done in Ref. 15, such possibility can be checked by extracting the temperature dependency and frequency dependency of relaxation time via an analysis of loss dynamics using, e.g., Cole-Cole formula loss.[17] Such analysis, to be accurate, requires the investigation of ε' and ε'' under a range of frequency that is much wider than the one available for the present study.

V. CONCLUSIONS

In summary, we combined measurements with first-principles-based techniques to investigate the low-temperature properties of $BaZrO_3$. This system is found to be cubic and macroscopically paraelectric down to 2 K. Unlike the "better-studied" $KTaO_3$[33,42] and $SrTiO_3$[16,29] incipient ferroelectrics, the zero-point vibrations do *not* suppress ferroelectricity in $BaZrO_3$. In other words, this latter material is also paraelectric in the classical regime. On the other hand, quantum effects lead to the saturation of the cubic lattice parameter below $\simeq$40 K.

Despite having no long-range-order structural phase transition, $BaZrO_3$ exhibits the following striking dielectric features: (1) the ε' real part of the dielectric response saturates in overall at low temperature (namely, below $\simeq$40 K) to a value $\simeq$50. Our PI-QMC simulations are in rather good agreement with experimental data, and show that such saturation is caused by zero-point vibrations; (2) the temperature behavior of ε' can be well fitted by the empirical Barrett relation when allowing the B parameter to differ from zero in this fit; (3) two peaks or fine structures are observed in ε' around 50–65 K and 15 K, respectively. The first peak shifts to lower temperatures when decreasing the frequency, while the second one occurs at around the same temperature but decreases in magnitude when decreasing the frequency; (4) these two fine structures are associated with anomalies in the imaginary part of the dielectric response, ε'', which peaks at around 45–60 K while suddenly and continuously increases when decreasing temperature below 20 K.

By comparing with previously reported data in other perovskites and adopting some related interpretations, we propose that the highest-temperature dielectric anomalies are caused by defects like oxygen vacancies and/or unavoidable impurity ions such as Fe^{3+}—which, e.g., are the source of free charge carriers, that can interact with a soft lattice to create a polaronic state responsible for the dielectric anomaly.[15] Furthermore, our (direct) first-principles calculations suggest that the lowest-temperature dielectric anomalies may result from local rotation of the oxygen octahedra.

In order to acquire a deeper knowledge of perovskites, it is interesting to compare items (1)–(4) with corresponding features in $KTaO_3$ and $SrTiO_3$. For instance, ε' also saturates at low temperature in $KTaO_3$ and $SrTiO_3$, but with a much higher value of the plateau (as a result of the quantum-induced *suppression* of ferroelectricity in these latter compounds). Such high value of the plateau explains why the B coefficient is generally omitted in the Barrett fit of $KTaO_3$ and $SrTiO_3$. It is also highly plausible, as we believe it, that such high ε' prevents the observation of the hump that should be associated (according to the Kramers-Kronig relation[17]) with the peak of ε'' seen around 30–50 K in $KTaO_3$[14,15] and $SrTiO_3$.[15,16]

We hope that our work stimulates further investigations aimed at checking our suggestions, in particular, and understanding dielectric anomalies in perovskites, in general.

ACKNOWLEDGMENTS

The authors would like to thank Jorge Íñiguez and David Vanderbilt for providing the code for PI-QMC simulations. This work is supported by ONR Grants N 00014-01-1-0365 (CPD), N00014-97-1-0048, N00014-04-1-0413 and 00014-01-1-0600, by NSF Grants DMR-0404335 and DMR-9983678 and by DOE Grant DE-FG02-05ER46188.

---

[1] P. S. Dobal, A. Dixit, R. S. Katiyar, Z. Yu, R. Guo, and A. S. Bhalla, J. Appl. Phys. **89**, 8085 (2001).

[2] Abdul-Majeed Azad and S. Subramaniam, Mater. Res. Bull. **37**, 85(2002); Mater. Res. Bull. **37**, 11 (2002).

[3] Abdul-Majeed Azad, S. Subramaniam, and T. W. Dung, J. Alloys Compd. **334**, 118 (2002).

[4] B. Robertz, F. Boschini, R. Cloots, and A. Rulmont, Int. J. Inorg. Mater. **3**, 1185 (2001).

[5] N. Lecerf, S. Mathur, H. Shen, M. Veith, and S. Hüfner, Scr. Mater. **44**, 2157 (2001).

[6] G. Taglieri, M. Tersigni, P. L. Villa, and C. Mondelli, Int. J. Inorg. Mater. **1**, 103 (1999).

[7] E. Celik, Y. Akin, I. H. Mutlu, W. Sigmund, and Y. S. Hascicek, Physica C **382**, 355 (2002).

[8] M. Koopman, S. Duncan, K. K. Chawla, and C. Coffin, Composites, Part A **32**, 1039 (2001).

[9] J. Brzezińska-Miecznik, K. Haberko, and M. M. Bucko, Mater. Lett. **56**, 273 (2002).

[10] L. Chai, M. A. Akbas, P. K. Davies, and J. B. Parise, Mater. Res. Bull. **32**, 1261 (1997).

[11] A. Erb, E. Walker, and R. Flükiger, Physica C **245**, 245 (1995).

[12] K. Tanaka, K. Suzuki, D. Fu. K. Nishizawa, T. Miki, and K. Kato, Key Eng. Mater. **269**, 57 (2004).

[13] P. K. Davies, in *Proceedings of the Symposium on Materials and Preocessing for Wireless Communications*, edited by T. Negas [J. Am. Ceram. Soc. **53**, 137 (1994)].

[14] B. Salce, J. L. Gravil, and L. A. Boatner, J. Phys.: Condens. Matter **6**, 4077 (1994).

[15] O. Bidault, M. Maglione, M. Actis, M. Kchikech, and B. Salce, Phys. Rev. B **52**, 4191 (1995).

[16] R. Viana, P. Lunkenheimer, J. Hemberger, R. Böhmer, and A. Loidl, Phys. Rev. B **50**, 601 (1994).

[17] B. K. P. Scaife, *Principles of Dielectrics* (Clarendon Press, Oxford, 1989).

[18] The ABINIT code is a common project of the Universite Catholique de Louvain, Corning, Inc., and other contributors (URL http://www.abinit.org)

[19] M. Teter, Phys. Rev. B **48**, 5031 (1993).

[20] P. Hohenberg and W. Kohn, Phys. Rev. **136**, B864 (1964); W. Kohn and L. J. Sham, Phys. Rev. **140**, A1133 (1965).

[21] J. P. Perdew and A. Zunger, Phys. Rev. B **23**, 5048 (1981).

[22] D. M. Ceperley and B. J. Alder, Phys. Rev. Lett. **45**, 566 (1980).

[23] H. J. Monkhorst and J. D. Pack, Phys. Rev. B **13**, 5188 (1976).

[24] R. D. King-Smith and D. Vanderbilt, Phys. Rev. B **47**, R1651 (1993).

[25] D. Vanderbilt, Phys. Rev. B **41**, R7892 (1990).

[26] W. Zhong, D. Vanderbilt and K. M. Rabe, Phys. Rev. Lett. **73**, 1861 (1994); Phys. Rev. B **52**, 6301 (1995).

[27] N. Metropolis, A. W. Rosenbluth, M. N. Rosenbluth, A. H. Teller, and E. Teller, J. Chem. Phys. **21**, 1087 (1953).

[28] J. Íñiguez and D. Vanderbilt, Phys. Rev. Lett. **89**, 115503-1 (2002).

[29] W. Zhong and David Vanderbilt, Phys. Rev. B **53**, 5047 (1996).

[30] D. M. Ceperley, Rev. Mod. Phys. **67**, 279 (1995).

[31] A. Cuccoli, A. Macchi, G. Pedrolli, V. Tognetti, and R. Vaia, Phys. Rev. B **51**, 12369 (1995).

[32] V. M. Fuenzalida and M. E. Pilleux, J. Mater. Res., **10**, 2749 (1996)

[33] A. R. Akbarzadeh, L. Bellaiche, K. Leung, J. Ińiguez, and David Vanderbilt, Phys. Rev. B **70**, 054103 (2004).

[34] G. A. Samara, J. Phys.: Condens. Matter **15**, R367 (2003).

[35] G. Samara, and B. Morosin, Phys. Rev. B **8**, 1256 (1973).

[36] Y. Zhao and D. J. Weidner, Phys. Chem. Miner. **18**, 294 (1991).

[37] S. Tinte, J. Íñiguez, K. M. Rabe, and D. Vanderbilt, Phys. Rev. B **67**, 064106 (2003).

[38] W. Zhong and David Vanderbilt, Phys. Rev. Lett. **74**, 2587 (1995).

[39] Note that using the LDA lattice constant of 7.8475 Bohr gives a frequency of -62.95 cm^{-1} for the R-point instability, to be com-

pared with the value of -40.63 cm^{-1} corresponding to the experimental lattice constant (equal to 7.9194).

[40] H. Stetson and B. Schwartz, J. Am. Ceram. Soc. **44**, 420 (1961).

[41] Dielectric constants at different temperatures are typically calculated using the correlation function method. However, for some temperatures and in order to get better statistics and smoother curves, we also used the difference between polarization under different electric field to extract the dielectric constant. These two kinds of methods provide similar results. For instance, in PI-QMC at $T=75$ K, the correlation function approach yields a value of 48.75 for the real part of the dielectric constant, while on the other hand the finite difference method leads to 49.48 when the electric field along either of x, y, or z directions is gradually increased from zero to 5×10^6 V/m.

[42] G. Samara, in *Solid State Physics*, edited by H. Ehrenreich and F. Spaepen (Academic Press, New York, 2001), Vol. 56, p. 239.

[43] J. Dec and W. Kleemann, Solid State Commun. **106**, 695 (1998).

[44] Note that the computed value of ε_∞ is mostly unchanged when using the LDA lattice constant (for which ε_∞ was theoretically found to be 4.912) or the experimental lattice constant (for which ε_∞ was theoretically found to be 4.928).

[45] J. H. Barrett, Phys. Rev. **86**, 118 (1952).

[46] C. Ang, A. S. Bhalla, and L. E. Cross, Phys. Rev. B **64**, 184104 (2001).

[47] G. A. Samara and, L. Venturini, in *First-Principles Calculations for Ferroelectrics: Fifth Williamsburg Workshop*, edited by R. E. Cohen and P. Gehring (IOP, Bristol, 2004), p. 122.

[48] V. V. Laguta, M. D. Glinchuk, I. P. Bykov, J. Rosa, L. Jastrabík, M. Savinov, and, Z. Trybula, Phys. Rev. B **61**, 3897 (2000).